A NEW TEST FACILITY FOR EVALUATION OF PARAMETERS DEFINING NOZZLE GUIDE VANE ENDWALL HEAT TRANSFER

Frank Rubensdörffer
Siemens Industrial Turbomachinery AB
Dept. of Research and Development
SE-61283 Finspong, Sweden

Torsten H. Fransson
The Royal Institute of Technology
Chair of Heat and Power Technology
SE-100 44 Stockholm, Sweden

ABSTRACT

A new test facility has been built at Siemens in Finspong for aero- and thermodynamic investigation of the parameters defining nozzle guide vane endwall heat transfer.

The overall objective of the work is to evaluate the heat transfer pattern on a master configuration endwall of a nozzle guide vane, which is used to validate a 3D Navier-Stokes CFD flow field and heat transfer calculation.

The test rig consists of a linear cascade with 4 upscaled vanes. It is operated at low pressure and low temperature while retaining realistic engine Mach and Reynolds numbers. The two middle vanes are instrumented with pressure taps around the midspan section. Also the hub endwall is instrumented with pressure taps to monitor the pressure distribution.

For the heat transfer tests the hub endwall is equipped with a thin-film heater foil. The tip endwall is equipped with four sapphire glass viewports to provide optical access to the heated hub endwall for an infrared camera. Also the leading edge of the middle vanes are equipped with thermocouples to control the approaching thermal boundary layer.

The design of the test facility, the measuring and evaluation techniques for endwall heat transfer with its advantages and limitations are discussed.

INTRODUCTION

Modern industrial gas turbines have to match the requirements of an increasing efficiency combined with very low emissions in a robust, cost-effective manner. To achieve those contradictory goals very high turbine inlet temperatures are used in combination with modern dry low NO_X burners. Those burners are often convective cooled, so that almost all air from the compressor goes through the burner. This minimizes the difference between the medium and the maximum turbine inlet temperature. This leads to a rather flat turbine inlet temperature profile compared to a jet engine, which have a more parabolic turbine inlet temperature profile. That means that the nozzle guide vane endwall heat load for an industrial gas turbine is much higher compared to a jet engine.

Therefore there is a need to find an optimum for the parameters defining nozzle guide vane endwall heat transfer. Numerous studies have been carried out previously which investigate the influence of the flow field parameters like Reynolds number (Goldstein and Spores (1988), Boyle and Russell (1989), Giel et al. (1996), Kang et al. (1998)), Mach number (Kumar et al. (1985), Perdichizzi (1989), Harasgama and Wedlake (1990), Harvey et al. (1998)) and turbulence intensity (Giel et al. (1996), Radomsky and Thole (2000)) on the nozzle guide vane endwall heat transfer but all leave the geometrical parameters unchanged.

One major geometrical parameter is the flow path before the nozzle guide vane consisting of the end of the combustion chamber and the interface between the combustion chamber and the nozzle guide vane. Another major geometrical parameter is the flow path through the nozzle guide vane defined by the endwall geometry, the airfoil design and the number of airfoils (pitch).

The objective with the new test rig presented in this study is to investigate the influence of the geometrical parameters on the nozzle guide vane endwall heat transfer.

NOMENCLATURE

A_{heat}	Area of heater foil	m^2
k	heat transition coefficient	W/m^2K
L_C	chord length	m
Ma	Mach number	-
Nu	Nusselt number	-
p_{stat}	static pressure	N/m^2
p_{tot}	total pressure	N/m^2
q_{conv}	convective heat flux	W/m^2
q_{cond}	conductive heat flux	W/m^2

q_{ele}	electric heat flux	W/m^2
q_{rad}	radiative heat flux	W/m^2
Q_{heat}	power of heater foil	W
s	airfoil surface distance	m
smax	total airfoil surf. distance	m
T_W	wall temperature	K
T_∞	bulk temperature	K

Greek

α	convective heat transfer coefficient W/m^2K	
δ_{per}	thickness of perspex	m
δ_{sty}	thickness of styrofoam	m
ε	surface emissivity	-
κ	ratio of specific heat	-
λ	thermal conductivity	W/mK
λ_{per}	thermal conductivity of perspex	W/mK
λ_{sty}	thermal conductivity of styrofoam	W/mK
σ	Stefan-Boltzmann constant $\sigma=5.67 * 10^{-8} W/m^2K^4$	

DESCRIPTION OF THE TEST FACILITY

As illustrated in Figure 1, the test facility consists of a diffusor, which is 1000 mm long and increases the inlet diameter from 340 mm to the outlet diameter of 500 mm.
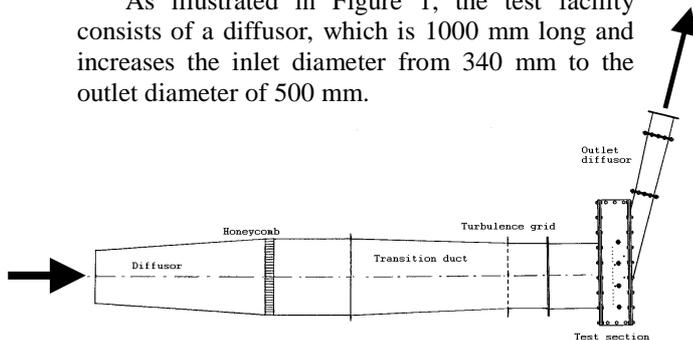
Figure 1: Schematic diagram of test facility

The diffusor is connected to the air supply of the laboratory workshop, which delivers up to 6 kg/s at a pressure of 1.5 bar in a temperature range between 20 to 40 °C. After the diffusor there is a honeycomb to settle the flow and to eliminate disturbances in the flow. Next follows a 1000 mm long transition duct, where the cross section changes smoothly from 500 mm circular to 436 mm * 574 mm rectangular in the flow direction. After the transition duct, 246 mm upstream of the test section a turbulence grid with 21 mm square openings and 6 mm bars is installed to increase the turbulence level. After the test section an outlet diffusor is installed to recover static pressure. The outlet diffusor is then connected to an exhaust stack. A photograph of the real test facility is shown in Figure 2.

Figure 2: Test facility

Test section and instrumentation

Figure 3 illustrates a schematic diagram of the test section.
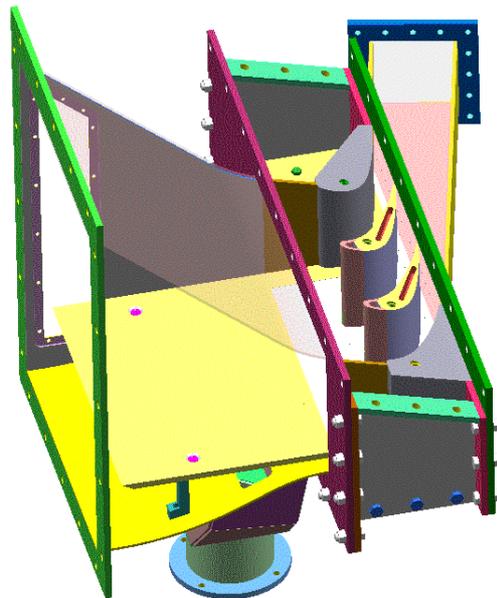
Figure 3: Schematic diagram of the test section

The test section consists of three parts: the inlet section, the airfoil section and the outlet section. It is a linear cascade with 4 airfoils and 3 flow passages. The airfoils are scaled up by a factor of two from a nozzle guide vane from a modern industrial gas turbine. The hub endwall in the inlet section is planar sized two times the airfoil chord length. Beneath the hub endwall an adjustable boundary layer bleed is employed to secure a parallel approaching flow field with a new boundary layer. A trip wire is installed at the beginning of the hub endwall to insure a uniform turbulent boundary layer on the hub endwall. The tip endwall is formed like the end of a real dry low NO_x combustion chamber.

2

The left side wall is equipped with a window to provide optical access to the inlet section of the investigated area of the test section, e.g. for laser measurements or facilitating the installation and alignment of aerodynamic probes.

There are two versions of the hub and tip endwall, one for the aerodynamic and the other for the heat transfer tests. For the aerodynamic tests the hub endwall is instrumented with 76 static pressure taps, see Figure 4, the tip endwall with 32 static pressure taps.
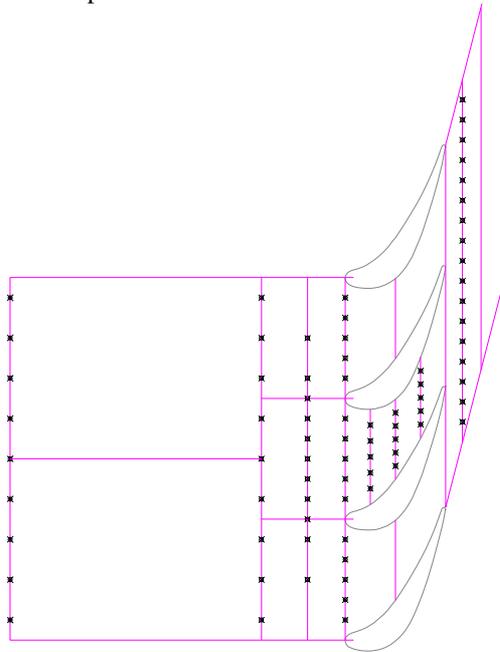
Figure 4: Hub endwall pressure tap distribution for aerodynamic tests.

For the heat transfer tests the number of the static pressure taps in the hub endwall is reduced to 35, which are placed in the inlet section upstream of the airfoil section and in the outlet section immediately downstream of the airfoil section. The hub endwall is equipped with a thin film foil heater in the airfoil section, see Figure 5. In the area where the thin film foil heater is installed the bearing perspex plate thickness is reduced from 10 mm to 3 mm. The remaining space is filled up with 7 mm styrofoam with a very low thermal conductivity ($\lambda = 0.030$ W/mK) to reduce the influence of the heat transfer through the plate by conduction. Two calibrated thermocouples are installed on the heater foil for calibration of the infrared camera temperature measurements.

The tip endwall in the airfoil section for the heat transfer tests is equipped with four viewports with sapphire glass to have optical access for an infrared camera to the heated hub endwall, see Figure 6. Production and cost limitations prevented the use of a single, continuous sapphire glass viewport, which has avoided the disadvantages of the viewport frames.
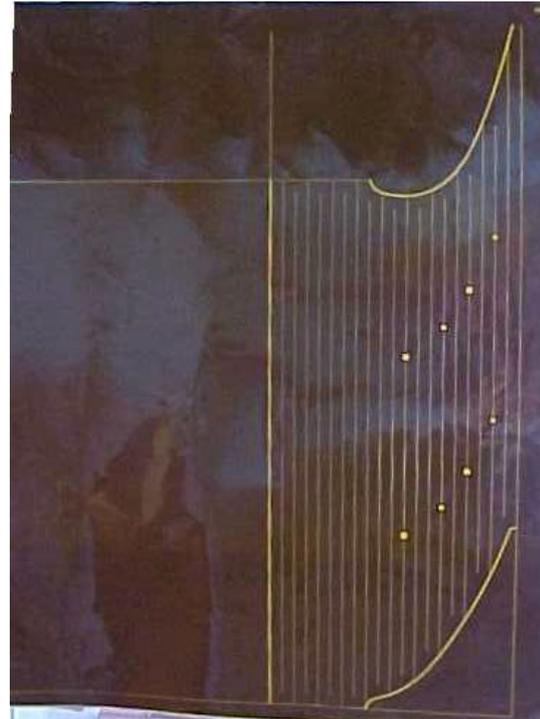
Figure 5: Thin film foil heater

Figure 6: Tip endwall with sapphire glass viewports

The two airfoils in the middle of the airfoil section are each instrumented with 14 static pressure taps in the midspan section and 10 thermocouples at the leading edge, see Figure 7.

An aerodynamic probe to measure the total inlet pressure upstream is utilized at the beginning of the test section. A 3-hole probe can be inserted in front of the knife-edge of the hub endwall to control the amount of purge air through the boundary layer bleed.

3

Figure 7: Instrumented airfoils

The outer hub endwall of the inlet section is also formed like the end of a real dry low NO_x combustion chamber, which can be used to replace the plane endwall with little adjustments in the future. Thus the rig can be used to test real engine geometries after a conversion.

The contour of the outlet section has been designed with the help of 3D-CFD calculations to secure that the flowfield through the three flow passages has a good periodicity without the use of adjustable tailboards.

The complete test section is painted black in order to obtain a high, constant surface emissivity.

MEASUREMENT AND DATA ACQUISITION

Two kinds of measurements are carried out in the described test facility: aerodynamic tests and heat transfer tests.

The aerodynamic tests are intended for the measurements of the pressure distribution on the hub and tip endwall and on the two profiles, the control and examination of the periodicity of the flow through the cascade and the adjustment of the boundary layer bleed flow.

The mass flow from the laboratory workshop supply to the rig is measured by a v-cone from Mc Crometer's. The mass flow through the cascade is adjusted so that the pressure drop over the cascade agrees as much as possible with the real engine conditions.

The mass flow through the boundary layer bleed is measured by an orifice plate according to ISO 5167-1. It is adjusted so that the approaching flow is parallel flow to the plane hub endwall.

The pressure taps are connected to the PSI pressure measurement system. The thermocouples for temperature measurements are connected to the analog/digital converter system Datascan.

All incoming data are logged by the Scadapro data logging system, which is used to review the data, check trends and extract average values for interesting time periods as a data file for further evaluation with Excel.

For online monitoring the temperature and pressure measurements from the Scadapro logging system are implemented into Excel datasheets with DDE- links. That means, that all important measurands for the rig like pressure distributions, temperature distributions and all other deduced parameters like Mach number distributions, mass flows, pressure ratios can be monitored and controlled online.

For the heat transfer tests there are two additional measurement equipments: an infrared camera Thermovision 900 system, see Agema 1994, to measure the surface temperature on the hub endwall and a wattmeter Yokogawa WT 110 to measure the heat flow of the thin film foil heater. The temperature images, which are taken by the IR camera, are saved in a matrix form in a chosen number of pixels. The complete measurement setup can be seen in Figure 8.
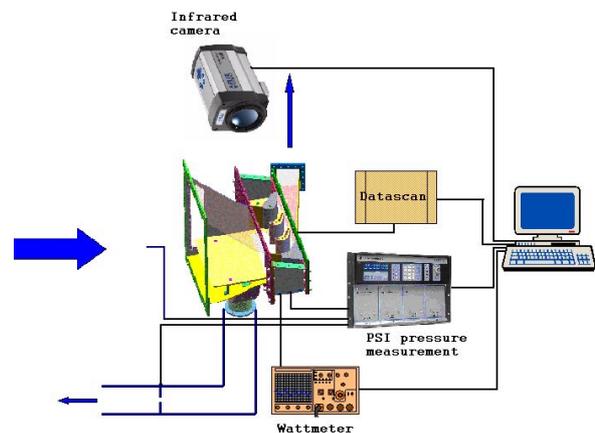
Figure 8: Measurement setup

DATA EVALUATION

The pressure measurements on the airfoil are used to calculated the Mach number distribution around the airfoil:

$$Ma = \sqrt{\frac{2}{\kappa-1}\left[\left(\frac{p_{tot}}{p_{stat}}\right)^{\frac{\kappa-1}{\kappa}} - 1\right]}$$

The main mass flow and the boundary layer bleed mass flow are calculated from the pressure measurements. All other data like pressure distribution on the tip and hub endwall and the temperature measurements in the leading edge are saved as raw. All data is saved in Excel worksheets.

The infrared images of the heated hub endwall, which have been take with the IR-camera, can be extracted as data files. Because of the frames for the sapphire glasses in the tip endwall and the limited optical access to the hub endwall several IR-images have to be taken from different optic angles but from the same distance to the hub endwall, see Figure 9.
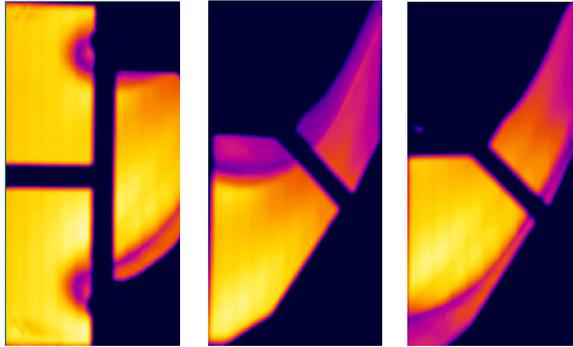
Figure 9: Leading edge-, suction side- and pressure side-area infrared image
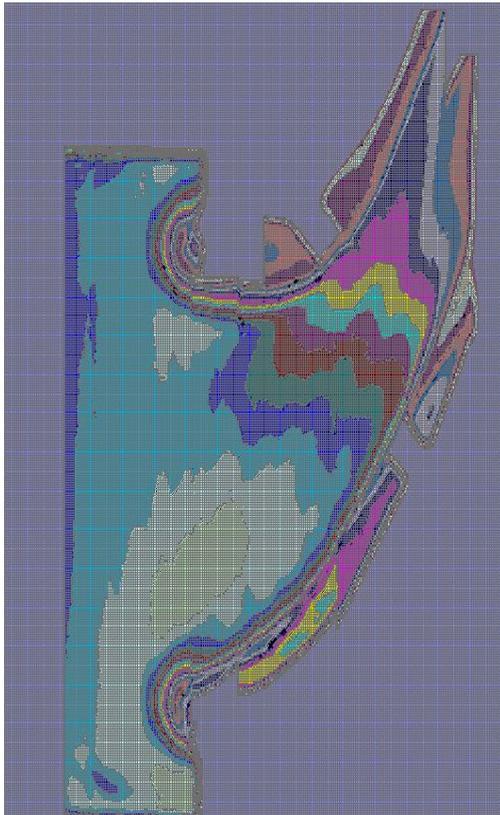
Figure 10: Complete hub endwall temperature distribution in Excel

These images are later combined to form a single composite image. This processing is done with the help of Excel, which provides good graphic and handling tools for the treatment of large data arrays. For the correct combing of the images it is important to have well defined reference point, like thermocouples, leading edges or other characteristic points, which can be optical recognizes easily to get a optimum complete image of the hub endwall temperature distribution, see Figure 10.

The final temperature data file is imported into Matlab for further evaluation.

The measured hub endwall temperature distribution is used to evaluate the non-dimensional hub endwall heat transfer distribution, which is defined by:

$$Nu = \frac{\alpha * L_C}{\lambda}$$

where the convective heat transfer coefficient α is defined as:

$$\alpha = \frac{q_{conv}}{T_W - T_\infty}$$

The convective heat flux q_{conv} can be calculated by:

$$q_{conv} = q_{ele} - q_{rad} - q_{cond}$$

where q_{ele} is defined by

$$q_{ele} = \frac{Q_{Heater}}{A_{Foil}}$$

q_{rad} is the radiation heat transfer from the heater foil to the surrounding rig:

$$q_{rad} = \sigma * \varepsilon * \left(T_W^4 - T_\infty^4\right)$$

where it is assumed that all surrounding surfaces are uniform at T_∞.

q_{cond} is conductive heat transfer through the perspex/styrofoam hub endwall:

$$q_{cond} = k\left(T_W - T_\infty\right)$$

with

$$k = \frac{1}{\dfrac{\delta_{per}}{\lambda_{per}} + \dfrac{\delta_{sty}}{\lambda_{sty}}}$$

These calculations are done in Matlab for the complete surface temperature matrix. This leads to the Nusselt number distribution on the hub endwall.

ACCURACY OF MEASUREMENTS AND UNCERTAINTY ANALYSIS

Considering typical values for the surface and the surrounding temperature shows, that the rate of the radiation heat flux to the total heat flux is around 3.7 % and the rate of the conductive heat transfer through the wall to the total heat flux around 2.1 %. Thus it appears that the chosen measurement method is well applicable for the measurement task.

An uncertainty analysis has been performed for the pressure and the heat transfer measurements. The maximum uncertainty was derived by the method of linear error propagation based on the first Taylor series, see Coleman and Steele, 1999.

For the Mach number a maximum uncertainty of 2 % was found. For the heat transfer the maximum uncertainty is lower than 6 %. There the uncertainty in the temperature difference measurement has the largest influence on the overall uncertainty.

PRELIMINARY RESULTS AND COMPARISION TO CFD CALCULATION

Figure 11 shows the measured Mach number distribution around the left and right airfoil in comparison to the CFD calculation in midspan section. On pressure side there is good agreement between the measurements and the CFD calculation. At the end of the airfoil the measurements show a slight deviation of the periodicity up to $\Delta Ma = 0.08$. Also on the suction side there is a rather good agreement between the measurements and the calculation.
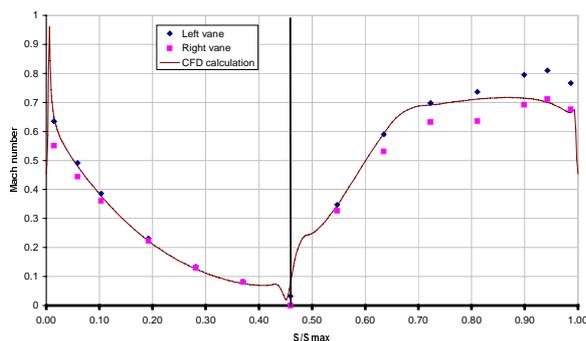
Figure 11: Measured and calculated Mach number distribution around profile midspan

On suction side the deviation of the periodicity starts already in the middle of the profile and reaches a maximum of $\Delta Ma = 0.10$. These deviations are caused by the design of the outlet section and the design of the outlet diffusor. The achieved periodicity of the flowfield in the rig with its deviations is judged to be applicable for the tests

and the evaluation of heat transfer to the hub endwall because the deviation in the flowfield starts rather downstream in the flow path and therefore effects only minor parts of the end of the hub endwall. Previous studies (Kumar et al. (1985), Perdichizzi (1989), Harasgama and Wedlake (1990), Harvey et al. (1998)) also show that the exit Mach number has only a minor impact on the endwall heat transfer. Therefore no changes or adjustments of the outlet section or the outlet diffusor are deemed to be necessary. These are very time consuming and normally give rather little improvement on the periodicity.

In Figure 12 and Figure 13 the measured and calculated endwall heat transfer can be seen.
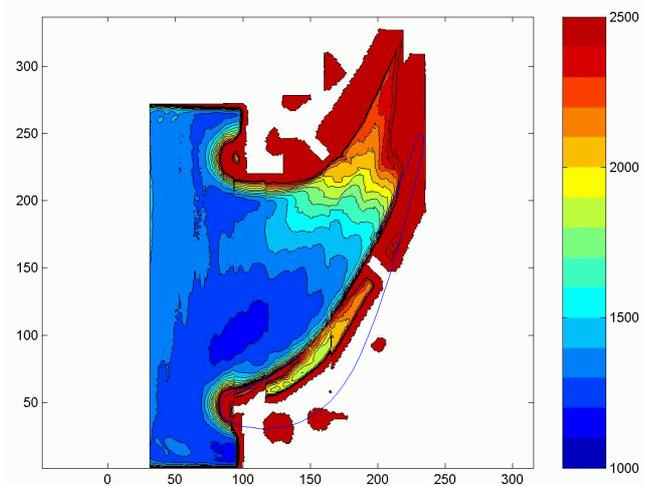
Figure 12: Measured hub endwall heat transfer distribution
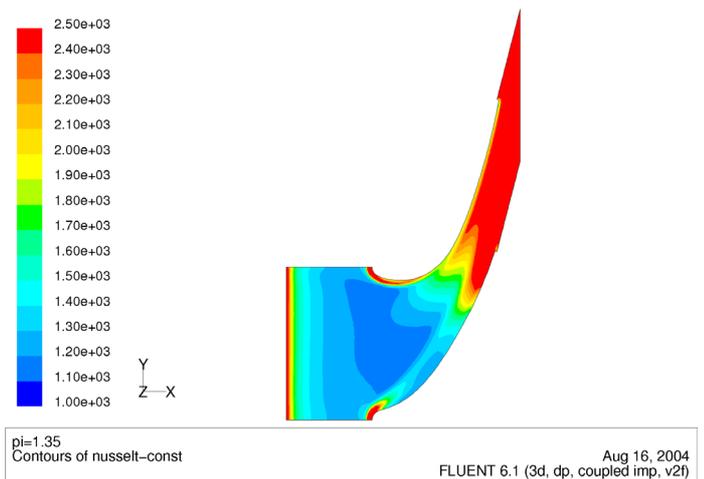
Figure 13: Calculated hub endwall heat transfer distribution

The comparison shows a very good agreement between the measurements and the CFD calculation regarding both the qualitative heat transfer pattern as well as the quantitative values of the heat transfer. In detail following features in the

6

endwall heat transfer pattern can be recognized both in the measurements and in the calculation: high heat transfer in the leading edge region caused by the horseshoe vortex, increasing heat transfer in the mean flow path due to flow acceleration and higher heat transfer on the suction side half of the endwall (half moon shape) compared to the pressure side half. However, the higher heat transfer streak in the vicinity of the pressure side caused by the pressure side leg of the horseshoe vortex is not so distinct in the measurements as in the calculation. This is probably caused by the conductive heat transfer through the bearing endwall plate for the heater foil, which dilutes sharp temperature gradients whereas the calculation assumes perfect adiabatic wall under the heater foil as boundary condition.

FURTHER DEVELOPMENTS

In Figure 14 – Figure 16 the future geometric variants, which can be implemented in the rig, are presented. In the first variant the plane hub inlet section from the master geometry is by the shape of the design of a real dry low NO_X combustion chamber. In the second variant a heat shield is implemented in front of the vane. This is a common design feature in industrial gas turbines. The heat shield can be operated with and without cooling air. The third variant includes a cavity in front of the vane. Those cavities are implemented in real gas turbines to compensate the different movements of combustion chamber and nozzle guide vane in transient operation conditions. Also this variant can be tested with and without cooling air.
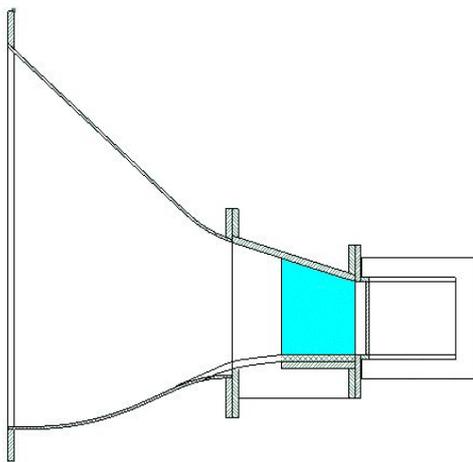
Figure 14: Dry low NO_X combustion chamber design
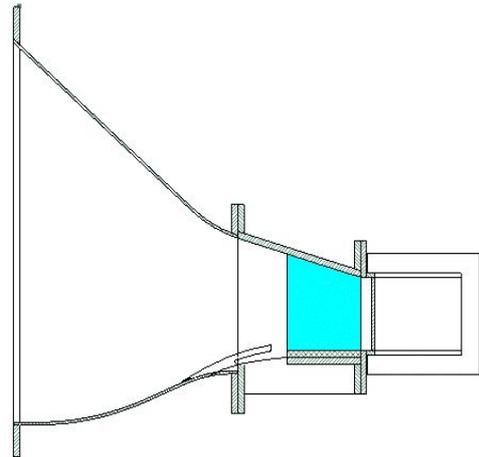
Figure 15: Combustion chamber and heat shield design
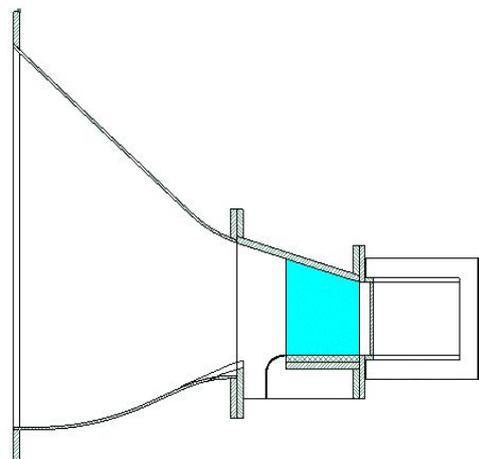
Figure 16: Combustion chamber and cavity design

In the existing setup the heat conductivity in the endwall dilutes sharp temperature gradients. A follow-on investigation will focus on identifying more suitable low heat conductivity material for the bearing endwall plate for the heater foil, which gives an equivalent physical load bearing capacity like the existing design.

CONCLUSIONS

A new test facility for aero- and thermo-dynamic investigations of nozzle guide vanes has been designed, manufactured, assembled and commissioned. The first tests showed that the cold low pressure rig is a reliable tool for the investigation of nozzle guide vane endwall heat transfer. The achieved accuracy is good. Also there is a good agreement between the measurements and CFD calculations concerning the flow field and the hub endwall heat transfer.

REFERENCES

Agema Thermovision 900 Series, 1994
Users' Manual, Agema Infrared Systems AB, Rinkebyvägen 19, Box 3, SE-18211 Danderyd, Sweden.

Boyle, R. J. and Russell, L. M.; 1989
"Experimental Determination of Stator Endwall Heat Transfer", ASME Paper No. 89-GT-219, ASME Journal of Turbomachinery, Vol. 112, pp. 547-558.

Coleman, H. W. and Steele, W. G.; 1999
"Experimentation and Uncertainty Analysis for Engineers", John Wiley and Sons, Inc, New York, ISBN: 0471121460

Giel, P. W., Thurman, D. R., Van Fossen, G. J., Hippensteele, S. A. and Boyle, R. J.; 1996
"Endwall Heat Transfer Measurements in a Transonic Turbine Cascade", ASME Paper No. 96-GT-180, ASME Journal of Turbomachinery, Vol. 120, pp. 305-313.

Goldstein, R. J. and Spores, R. A.; 1988
"Turbulent Transport on the Endwall in the Region Between Adjacent Turbine Blades", ASME Journal of Heat Transfer, Vol. 110, pp. 862-869.

Harasgama, S. P. and Wedlake, E. T.; 1990
"Heat Transfer and Aerodynamics of a High Rim Speed Turbine Tested in a RAE Isentropic Light Piston Cascade (ILPC)", ASME Paper No. 90-GT-41, Brussels, Belgium.

Harvey, N. W., Rose, M.G. Coupland, J. and Jones, T. V.; 1998
" Measurements And Calculation of Nozzle Guide Vane End Wall Heat Transfer", ASME Paper No. 98-GT-66, ASME Journal of Turbomachinery, Vol. 121, pp. 184-190.

Kang, M. B., Kohli, A. and Thole, K.A.; 1998
"Heat Transfer and Flowfield Measurements in the Leading Edge Region of a Stator Vane Endwall ", ASME Paper No. 98-GT-173, ASME Journal of Turbomachinery, Vol. 121, pp. 558-568.

Kumar, G. N., Jenkins, R. M. and Sahu, U.; 1985
"Regionally Averaged Endwall Heat Transfer Correlations for a Linear Vane Cascade", ASME Paper No. 85-GT-19, Houston, Texas.

Perdichizzi, A.; 1989
"Mach Number Effects on Secondary Flow Development Downstream of a Turbine Cascade", ASME Paper No. 89-GT-67, Toronto, Ontario, Canada.

Radomsky, R. W. and Thole, K.A.; 2000a
"Flowfield Measurements for a Highly Turbulent Flow in a Stator Vane Passage", ASME Journal of Turbomachinery, Vol. 122, pp. 255-262.

Radomsky, R. W. and Thole, K.A.; 2000b
"High Freestream Turbulence Effects on Endwall Heat Transfer for a Gas Turbine Stator Vane ", ASME Paper No. 2000-GT-0201, Munich, Germany.